Appl. Phys. B 49, 545–552 (1989)

Applied Physics B Photophysics and Laser Chemistry

Experimental Test of a Four-Level Kinetic Model for Excited-State Intramolecular Proton Transfer Dye Lasers

A. Costela, J. M. Muñoz, A. Douhal, J. M. Figuera, and A. U. Acuña

Instituto de Química Física "Rocasolano", C.S.I.C. Serrano, 119, E-28006 Madrid, Spain

Received 29 March 1989/Accepted 4 July 1989

Abstract. The nanosecond pulses of a dye laser oscillator based on the excited-state intramolecular proton-transfer reaction (IPT) of salicylamide and 2'-hydroxylphenyl benzimidazole dyes have been studied as a function of several experimental parameters. To explain the operation of this laser a numerical four-level kinetic model was developed until the lasing properties of these dyes, in the presence of a variable oxygen concentration and pumped with a double pulse technique, could be reproduced. This was possible only by assuming that the efficiency of the laser is controlled by the absorption cross-section of a transient state with a lifetime in the nanosecond-picosecond range, which was tentatively identified as a ground state tautomeric species.

PACS: 33.50, 42.55M

Recently, a number of laser dyes have been described [1–5] where generation of stimulated radiation is due to a proton transfer photochemical mechanism. In brief, an intramolecular proton-transfer (IPT) reaction of the electronically excited molecule results in an excited product (tautomer) having zero concentration in the ground state and emitting fluorescence with a high yield and a large Stokes shift (6000–10000 cm^{-1}) [6–8]. This mechanism produces a large population inversion and we were able to demonstrate [2–4] efficient laser operation for a number of salicylic and benzimidazole derivatives (Schemes 1 and 2).

Lasing organic compounds based on the intramolecular proton-transfer reaction show a number of interesting properties compared with the more usual dyes [1–5]. For example, the wavelength of some of the most frequent pumping sources (N_2, excimers, Nd:YAG[3]) corresponds to the lowest singlet absorption of these dyes and therefore the photochemical decomposition might be minimized. However, several aspects of the lasing mechanism of proton-transfer dyes derived from salicylic and benzimidazole compounds are poorly understood, e.g. the relaxation processes leading to pulse termination and the loss terms determining the gain coefficient and wavelength distribution. Therefore a four-level model was developed to simulate numerically the temporal profile and gain distribution of these laser-pumped proton-transfer lasers with the aim of gaining insight into the kinetics of the laser. To determine the relative im-

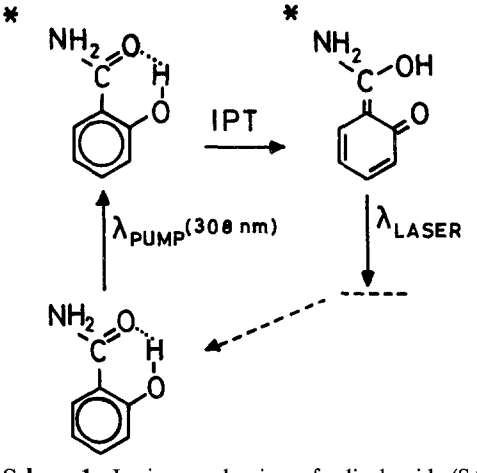

Scheme 1. Lasing mechanism of salicylamide (SAM)

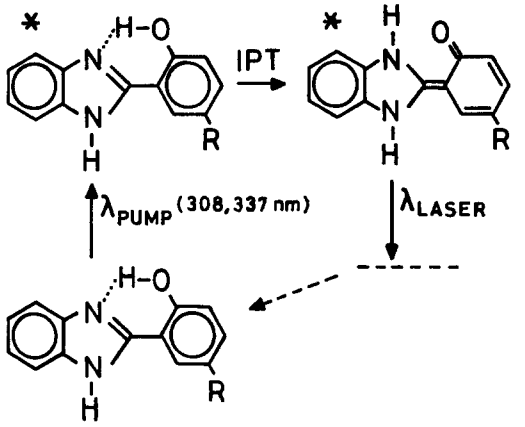

Scheme 2. Lasing mechanism of benzimidazoles. R=H: 2-(2′-hydroxyphenyl)benzimidazole (PBIM); R=OH: 2-(2′,5′-dihydroxyphenyl)benzimidazole (DI-PBIM); R=CH_3: 2-(2′-hydroxy-5′-methyl)benzimidazole (Me:BIM); R=OCH_3: 2-(2′-hydroxy-5′-methoxy)benzimidazole (OMe-BIM); R=F: 2-(2′-hydroxy-5′-fluoro)benzimidazole (F-BIM); R=Cl: 2-(2′-hydroxy-5′-chloro)benzimidazole (Cl-BIM)

portance of each process, we required the model to reproduce the outcome of several laser experiments, where we varied the oxygen concentration in the sample, the fluorescence quantum yield and lifetime of the dye, and the delay of a second pumping pulse. In this way a consistent kinetic picture of the laser was produced.

1. Experimental

Salicylamide (*o*-hydroxybenzamide) (Merck) was purified as described in [9]; 2-(2′-hydroxyphenyl) benzimidazole (PBIM) was prepared from phenilenediamine and salicylic acid as described previously [3]. The synthesis of the 5′-substituted derivatives of PBIM (Scheme 2) was carried out following essentially the same procedure and using the corresponding 5-derivative of salicylic acid. The purity of the dyes was checked by HPLC, TLC and combustion analysis. Spectroscopic quality N,N-dimethylformamide, methanol, acetonitrile and dioxane (Merck) were used as solvents without further purification. Absorption and emission spectra, fluorescence quantum yields and lifetimes of the dye solutions were measured as described elsewhere [10].

The IPT laser solutions were transversely pumped by 308 nm pulses from a home-made XeCl excimer laser [11]. The details of the laser system are described elsewhere [4]. In the double-pulse experiments the proton-transfer laser was pumped by pulses from two discharge-excited XeCl lasers triggered from a single spark-gap. Relative delays between the pulses could be introduced by varying the discharge circuitry. The laser solution was either saturated with oxygen (1 atm.) or degassed by bubbling with Ar (99.998%). The pump energy was 2–3 mJ focused on a stripe of 8×0.5 mm. The dye concentration was chosen so that the absorption is approximately 1 in 0.5 mm.

The dye and pump laser pulses were characterized with the following instruments: GenTec ED-100A and GenTec ED-200 energy meters, ITL TF 1850 fast rise-time photodiode, Tektronix 7912 AD transient digitizer, 7934 and 468 storage oscilloscopes, Bausch and Lomb 33-86-79 high-intensity monochromator, EMI 9763 B photomultiplier and a 6.35 mm thick solid etalon.

2. Results and Discussion

2.1. The Effect of Double Pulsing and Oxygen Concentration on the Laser Emission

Figure 1 displays the time profile of the laser pulses for dye solutions equilibrated in air. Typical intracavity photon flux was 1.27×10^{25} photons $cm^{-2} s^{-1}$ (PBIM) and 2.2×10^{25} photons $cm^{-2} s^{-1}$ (SAM). The pulses from PBIM and its derivatives follow closely the pulse shape of the XeCl pump pulse. In contrast, the laser pulse from salicylamide ends abruptly after 4 ns. This difference between the two dyes is also observed when the laser is pumped sequentially with two pulses with a variable delay, from 25 ns (to avoid overlapping) to 80 ns, and the oxygen concentration of the solutions is varied. Thus, when the solutions are deoxygenated, there is only a single laser pulse in SAM for any

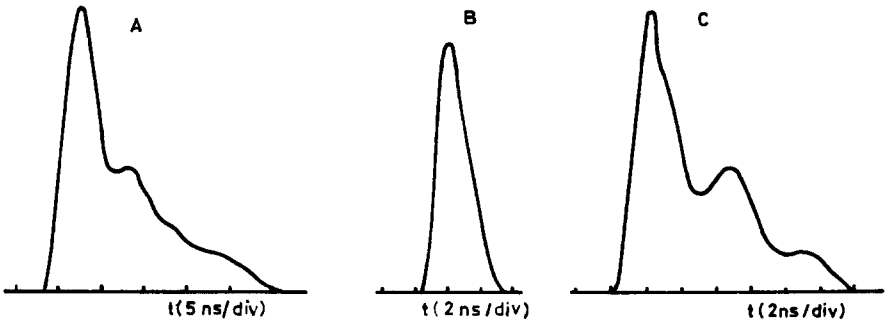

Fig. 1A–C. Experimental shapes of laser pulses. **A** The XeCl pump pulse (308 nm). **B** SAM in N,N′-dimethylformamide (443 nm). **C** PBIM in dioxane (473 nm)

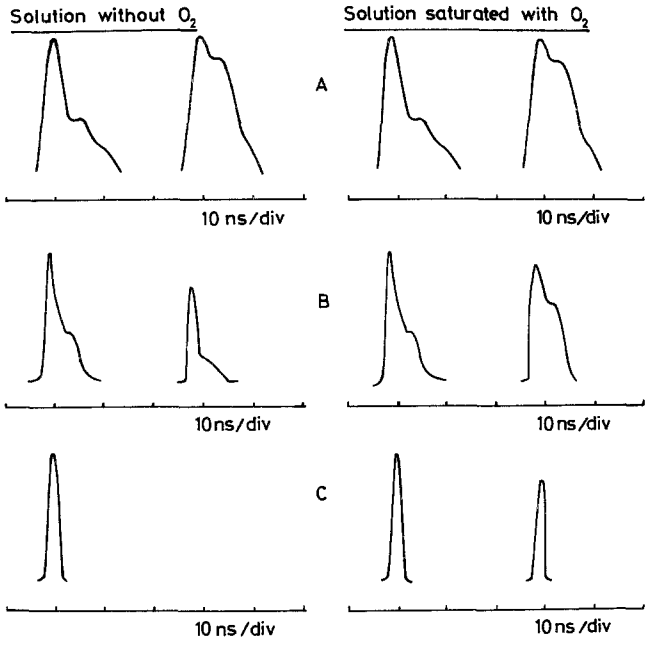

Fig. 2A–C. The dye laser emission, when pumped with a two pulse sequence, as a function of oxygen concentration. **A** The XeCl pump double pulse. **B** Lasing from PBIM in dimethylformamide. **C** Lasing from SAM in dimethylformamide

interpulse delay (Fig. 2) while in PBIM a second laser pulse can be always detected (Fig. 2), up to the maximum delay of system. The amplitude of the second pulse becomes smaller and the structure less defined as the delay increases. The same features are observed for a control solution of 2.5×10^{-3} M Rhodamine 6G in ethanol. To quantify these results we define a parameter E_2 representing the normalized energy of the second (delayed) laser pulse. This parameter is computed by taking the ratio of the energy of the laser pulse, when the dye is pumped with the two pulse sequency, to the energy of the laser pulse when the dye is pumped with a single pulse. The relationship between E_2 and the interpulse delay is presented in Fig. 3 for Rh 6G and PBIM.

When the dye solutions are fully saturated with oxygen a second pulse can be detected also in SAM (Fig. 2) for any delay between the two pumping pulses. In PBIM, and in Rh 6G, double lasing is also observed (Fig. 2) although in this case the shape and amplitude of the second pulse is constant for any delay (Fig. 3b). The O_2-dependent effects are interpreted (see below) as induced by the triplet states of the dyes.

2.2. *Kinetic Modelling of the IPT Laser*

The scheme of Fig. 4 summarizes the four-level kinetic model used here to formulate the set of differential rate equations of the IPT laser. It was developed from that first proposed by Kasha and coworkers [1, 12] to

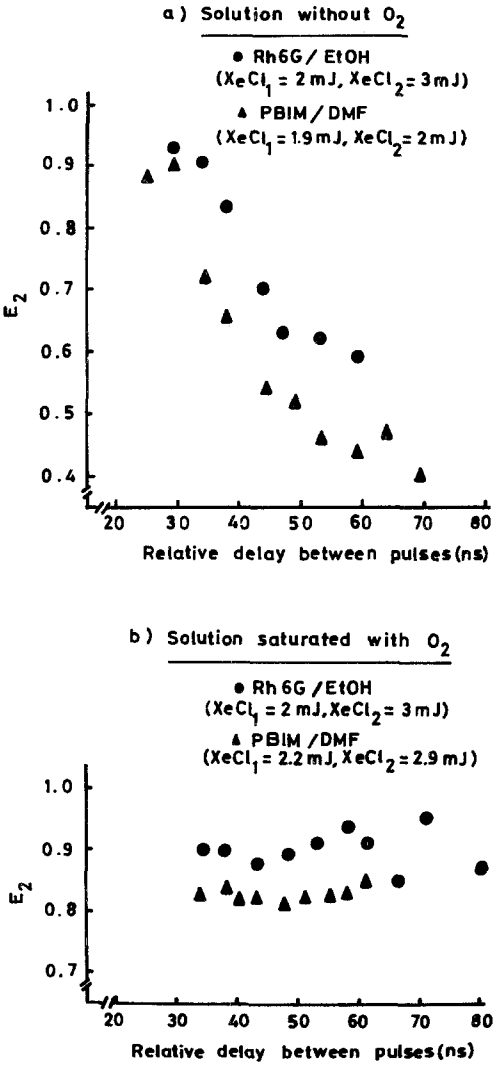

Fig. 3a, b. The relative energy of the delayed pulse of the dye laser (E_2) as a function of the interpulse delay of the pump. The data from Rh 6G/ethanol are included for comparison

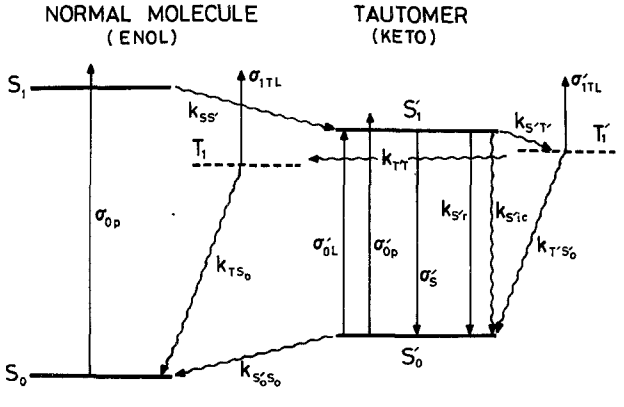

Fig. 4. The kinetic model of the intramolecular proton transfer laser. See Sect. 2.2 for notation

explain the lasing mechanism of intramolecular proton transfer dye and its essential features are the same as those used by Ernsting and Nikolaus [13] to model laser pulse shortening by excited state IPT. In Fig. 4 we represent states and parameters of the initial molecule (i.e. the *enol* or *normal* molecule) by umprimed symbols (S_0, S_1) while primed symbols (S'_0, S'_1) are used for the tautomeric species that is created by the proton-transfer reaction. Higher excited manifolds ($S_i, T_i, i>1$) are not shown since radiationless transitions back to S_1 (or T_1) are known to be fast ($10^{-12}-10^{-11}$ s) on the time scales of interest to us [14].

The notation is as follows

$k_{SS'}$: rate constant of the intramolecular proton-transfer in the excited singlet state.
$k_{S'_0S_0}$: back proton-transfer rate constant in the ground state.
$k_{T'T}$: back proton-transfer in the tautomer triplet state.
$k_{S'T'}$: intersystem crossing $S'_1 \rightarrow T'_1$.
$k_{T'S'_0}$: intersystem crossing $T'_1 \rightarrow S'_0$.
k_{TS_0}: intersystem crossing $T_1 \rightarrow S_0$.
$k_{S'_r}$: radiative transition $S'_1 \rightarrow S'_0$.
$k_{S'ic}$: internal conversion $S'_1 \rightarrow S'_0$.
σ'_S: stimulated emission cross section at laser wavelength.
σ'_{Op}: absorption cross section of S'_0 at pump wavelength.
σ'_{1TL}: absorption cross section for $T'_1 \rightarrow T'_n$ transitions ($n>1$) at laser wavelength.
σ'_{OL}: absorption cross section of S'_0 at laser wavelength.
σ_{Op}: absorption cross section of S_0 at pump wavelength.
σ_{1TL}: absorption cross section for $T_1 \rightarrow T_n$ transitions ($n>1$) at laser wavelength.
ϕ_F: tautomer fluorescence quantum yield.

The initial step is the absorption of pump radiation that gives rise, throught an excited-state proton (or H-atom) transfer reaction, to the formation of electronically excited tautomers (S'_1). We assume that this process, that usually occurs in the subpicosecond time interval (i.e. $k_{SS'} \simeq 10^{12}\,s^{-1}$), is irreversible and occurs with a 100% efficiency, as has been shown for methylsalicylate [15]. From the S'_1 state, the excited population is depleted by several radiative and non-radiative processes (Fig. 4) involving the triplet and singlet ground states of the tautomer and, to keep the model as general as possible, the triplet state of the normal molecule. All these transient states are considered initially as possible candidates for depressing the laser gain.

Those rate constants and cross-sections needed to solve the set of differential rate equations that were available experimentally [10] are collected in Table 1. The normalized fluorescence spectrum of the tautomer $\int_0^\infty E(\lambda)d\lambda \equiv \phi_F$ was used to determine the value of σ'_S from the expression:

$$\sigma'_S(\lambda) = \frac{\lambda^4 E(\lambda)}{8\pi c n^2 \tau'_r}, \tag{1}$$

where τ'_r is the radiative lifetime of the tautomer ($k_{S'_r}^{-1}$), n is the refractive index and c is the speed of light. The experimental values of the absorption coefficients ε (in $1\,mol^{-1}\,cm^{-1}$) of the initial (enol) species were translated to cross sections (cm^2/mol) by the factor 3.824×10^{-21}.

Table 1. Experimentally determined values[a]

Dye	Solvent[b]	σ_{Op} [cm^2]	ϕ_F	τ'_r[c] [ns]	τ'[d] [ns]	σ'_S [cm^2]	C [mole/l]
PBIM	DMF	6.3×10^{-17}	0.72	6	4.1	5.2×10^{-17}	1.9×10^{-3}
PBIM	d	6.8×10^{-17}	0.65	6	4.2	4.5×10^{-17}	1.7×10^{-3}
PBIM	an	4.3×10^{-17}	0.55	7	3.7	3.8×10^{-17}	2.5×10^{-3}
PBIM	MeOH	8.1×10^{-17}	0.57	7	3.8	3.5×10^{-17}	1.6×10^{-3}
F-BIM	an	4.9×10^{-17}	0.73	6	4.7	6.1×10^{-17}	1.5×10^{-3}
Cl-BIM	d	6.0×10^{-17}	0.65	8	5.2	3.7×10^{-17}	1.4×10^{-3}
Me-BIM	d	4.2×10^{-17}	0.65	7	4.5	4.1×10^{-17}	2.3×10^{-3}
OMe-BIM	d	2.7×10^{-17}	0.48	9	4.2	2.8×10^{-17}	3.3×10^{-3}
DI-PBIM	d	3.1×10^{-17}	0.39	9	3.4	2.5×10^{-17}	3.0×10^{-3}
DI-PBIM	an	2.2×10^{-17}	0.18	12	2.2	8.6×10^{-18}	4.0×10^{-3}
DI-PBIM	DMF	3.4×10^{-17}	0.21	12	2.6	9.3×10^{-18}	2.6×10^{-3}
SAM	DMF	1.6×10^{-17}	0.27	10	2.6	7.8×10^{-18}	5.8×10^{-3}

[a] Ref. [9, 10]
[b] DMF = dimethylformamide; d = dioxane; an = acetonitrile; MeOH = methanol
[c] S'_1 radiative lifetime: $1/\tau'_r = k_{S'_r}$
[d] S'_1 lifetime: $1/\tau' = 1/\tau'_r + k_{S'T'} + k_{S'ic}$

The tautomer absorption spectrum, which should be substantially shifted to the red of the normal molecule absorption, is unknown and therefore its absorption cross section at the pump wavelength had to be estimated. A value of $\sigma'_{Op}=\sigma'_S/10\,cm^2$ was used in all the computations here. As would be expected from kinetic considerations the final solutions of the model are not very sensitive to the value of σ'_{Op}.

The essential processes leading to the termination of the laser pulse might be the depopulation of S'_1 by non-radiative channels ($k_{S'T'}$ and $k_{S'ic}$) and the absorption of laser emission by transient states (T_1, T'_1, and S'_0). The losses due to triplet-triplet absorption are determined by the intersystem crossing rate and triplet lifetime, which are unknown for these compounds. It was initially assumed that in SAM all the radiationless processes depopulating S'_1 were connected with the triplet T'_1 and therefore $k_{S'T'}\simeq 3\times 10^8\,s^{-1}$ (from the data of Table 1), a value similar to that postulated [16] for the related IPT dye 2-(2'-hydroxyphenyl) benzothiazole, HBT. It was further assumed that the decay of the triplets was slow enough to prevent the formation of a second laser pulse after a pump delay of ~ 70 ns in the degassed SAM solution. When the solution is fully saturated with O_2, the triplet lifetime must be much shorter to explain the formation of a second pulse after a delay of only 25 ns. But in that case, if triplet losses were in fact the controlling step of the pulse termination, the faster depletion of the triplet population would give rise – according to this simple model – to a much longer first laser pulse than is actually observed. Hence, we assumed that O_2-independent process dominant in the first pulse shortening is the accumulation of ground state tautomers (S'_0) generated by direct internal conversion from S'_1, while the formation (but not the shape) of the delayed pulse depends mainly on the rate of triplet population. To estimate the initial fractional distribution of molecules between S'_0 and T'_1 states the ratio $k_{S'ic}/k_{S'T'}$ was set to the range of values (4 ± 3) that successfully reproduced the behaviour of the SAM solution as a function of O_2 concentration and number of pump pulses.

A similar reasoning was followed to explain the experimental behaviour of the PBIM solutions, that can be also modelled with values of the ratio $k_{S'ic}/k_{S'T'}$ of 4 ± 2. Although it is unlikely that this ratio would be identical for both kinds of dyes, a value of 4 was kept constant in all the numerical calculations reported here, taking into account the approximations involved in the model. Since from the data of Table 1 $k_{S'ic}+k_{S'T'}=8.3\times 10^7\,s^{-1}$ (PBIM in dioxane), this means that $k_{S'T'}\simeq 2\times 10^7\,s^{-1}$.

The decrease of the relative energy (E_2) of the delayed pulse in degassed solutions (Fig. 3) is probably the result of the accumulation of a small amount of photodecomposition products somehow related with the triplet formation, a possibility not included in the model. The low yields of triplet formation postulated here are not unexpected in molecules closely related with a family of compounds used industrially as photostabilizers. The very high photochemical stability of these substances showing IPT seems to be related to fast internal conversion rates that dissipate the absorbed electronic energy avoiding triplet formation [13].

The electron charge density distribution of triplet states makes energetically more stable an enol configuration [7], therefore the molecule might switch back from a keto (T'_1) to an enol (T_1) by a reverse proton transfer step, preserving the spin multiplicity. This reaction, that was proposed by Mordzinski and Grellman [17] to account for the formation of enol triplet states in the excited state IPT of 2-(2'-hydroxyphenyl) benzoxazole (HBO), should be much faster than the spin-forbidden intersystem crossing, i.e. $k_{T'T}\gg k_{T'S_0}$. Hence, we assumed here a similar situation and assign the value $10^9\,s^{-1}$ to $k_{T'T}$. The spin-forbidden transitions T_1 to S_0 (T'_1 to S'_0) are included with typical rate constants of $10^6\,s^{-1}$. In O_2-saturated solutions these rates are enhanced, shortening the triplet lifetime and if the process is controlled by diffusion (at unit collisional efficiency) then $k_{TS_0}(k_{T'S'_0})$ would take values close to $10^8\,s^{-1}$, which still is a factor of ten lower than $k_{T'T}$.

The absorption cross-section of the triplet states at the laser wavelength was postulated to be roughly equal to that of the keto ground state, i.e. $\sigma_{1TL}\simeq\sigma'_{1TL}\simeq\sigma'_{OL}$, by considering the (scarce) experimental data available for similar derivatives [18, 19] or dyes as Rh 6G. In the time range of the experiments described here, the precise value of $\sigma_{1TL}(\sigma'_{1TL})$ is uncritical.

The values of all the parameters discussed above that were not determined experimentally are collected in Table 2 and were kept constant throughout the computations. With these values and those of Table 1 a set of differential rate equations was formulated in the usual way, for pulsed operation at a laser wavelength in the maximum of the gain distribution. These rate

Table 2. Assumed values of fixed parameters

$k_{SS'}=10^{12}\,s^{-1}$
$k_{T'T}=10^9\,s^{-1}$
$\sigma'_{Op}=\sigma'_S/10$
$k_{S'ic}=4k_{S'T'}$
$k_{TS_0}=k_{T'S'_0}=10^8\,s^{-1}$. Solution saturated with O_2
$=10^6\,s^{-1}$. Solution without O_2
$\sigma_{1TL}=\sigma'_{1TL}=\sigma'_{OL}$

equations may be written as:

$$\frac{dN_0}{dt} = k_{S'_0S_0}N'_0 + k_{TS_0}N_T - \sigma_{Op}I_pN_0, \tag{2}$$

$$\frac{dN_1}{dt} = \sigma_{Op}I_pN_0 - k_{SS'}N_1, \tag{3}$$

$$\frac{dN_T}{dt} = k_{T'T}N'_T - k_{TS_0}N_T, \tag{4}$$

$$\frac{dN'_0}{dt} = (k_{S'r} + k_{S'ic})N'_1 + \sigma'_sI_LN'_1 + k_{T'S'_0}N'_T - \sigma'_{Op}I_pN'_0 - \sigma'_{OL}I_LN'_0 - k_{S'_0S_0}N'_0, \tag{5}$$

$$\frac{dN'_1}{dt} = k_{SS'}N_1 + \sigma'_{Op}I_pN'_0 + \sigma'_{OL}I_LN'_0 - \frac{1}{\tau'}N'_1 - \sigma'_SI_LN'_1, \tag{6}$$

$$\frac{dN'_T}{dt} = k_{S'T'}N'_1 - k_{T'T}N'_T - k_{T'S'_0}N'_T, \tag{7}$$

$$\frac{dI_L}{dt} = (cI_L/n)(\sigma'_SN'_1 - \sigma'_{OL}N'_0 - \sigma'_{1TL}N'_T - \sigma_{1TL}N_T) - (I_L/n\tau_c), \tag{8}$$

where N_0, N_1, N_T, N'_0, N'_1, N'_T are the population densities (molecule $\cdot$ cm^{-3}) of the S_0, S_1, T_1, S'_0, S'_1, T'_1 states, respectively; I_p, I_L are the pump and laser flux (photon cm^{-2} s^{-1}), respectively; τ' is the S'_1 lifetime, τ_c the cavity decay time, c the speed of light in vacuum and n the solution refractive index. The remaining symbols have been defined at the beginning of this section. The pump pulse used in these equations was the experimental one. The cavity decay time was $\tau_c = 125$ ps.

The numerical integration was done by a fourth-order Runge-Kutta routine. Initially only two quantities were allowed to take variable values until the experimental pulse shapes and double-pulse distribution of the IPT laser were reproduced: the absorption cross section of tautomer ground states (σ'_{OL}) and the rate of back proton transfer in the ground state manifold ($k_{S'_0S_0}$).

The precise meaning of the important parameter σ'_{OL} needs further elaboration. In the actual experimental conditions (fluid solutions at room temperature) the laser emission takes place from thermalized tautomer molecules in the lowest vibronic level of S'_1 to a set of vibronic sublevels of S'_0. Therefore, a more accurate representation of the energy-level diagram would be that of Fig. 5, where $S'_0(*)$ is just one of the several higher-lying vibrational states of S'_0 involved in the lasing process. In that case, one should specify the rate equation for each of these sub-levels, considering

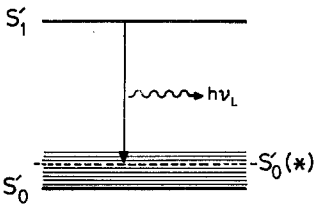

Fig. 5. Simplified energy level representation of the laser emission from the tautomer species

the possible transitions among them and their absorption of laser and pump radiation. However, the number of differential equations can be reduced considerably by recalling that the thermalization of the vibronically-excited ground-state tautomers is also much faster than any of the radiative steps involved in the process, as would be expected in our experimental conditions. Hence, a single rate equation is sufficient to describe the evolution of the total population N of S'_0. In this way, the absorption of the laser photon density (I_L) by ground state tautomers is described by the term $\sigma'_{OL}NI_L$, where σ'_{OL} is the absorption cross section of the tautomer thermalized in the S'_0 level at the laser wavelength.

The outcome of the model is very sensitive to the values of σ_{OL} and $k_{S'_0S_0}$, as expected, so the final values of these parameters (Table 3) can be considered as theoretical predictions for each of the laser dyes studied here.

It is important to note that the rate of back proton-transfer of the ground-state tautomer ($k_{S'_0S_0}$) can take values only within a very narrow interval, that is determined independently of σ'_{OL}. On the one hand, an upper limit is set by the condition $\sigma'_{OL} \leqq \sigma'_S$ (we are considering operation at a laser wavelength in the maximum of the gain distribution) while, on the other hand, values too small of $k_{S'_0S_0}$ would not be compatible with the generation of a nanosecond-delayed pulse in the double pulse experiments. Hence, the final model contains essentially a single free parameter (σ'_{OL}) that is chosen (Table 3) to reproduce the experimental laser pulse shape and width.

The agreement between the model results and experiment is very satisfactory. An example of that is shown in Fig. 6, where the modelled pulses were computed with the set of parameters from Tables 1–3. The initial spike preceeding the laser pulse is a numerical artefact of the integrating routine, due to the non-zero value of the proton laser flux in the short period near the laser onset [19].

As pointed out before, the experimental data only can be reproduced satisfactorily with a very limited range of values of σ'_{OL} and $k_{S'_0S_0}$. Thus, with a common value of $k_{S'_0S_0} = 1.5 \pm 0.15 \times 10^8$ s^{-1} the kinetic scheme accounts for the lasing behaviour of all the compounds

Table 3. Model predictions of adjustable parameters

Dye	Solvent[a]	σ'_{OL} [cm^2]	σ'_S/σ'_{OL}	
PBIM	DMF	2.0×10^{-17}	2.6	$k_{S_0S_0}=1.5\pm0.15\times10^8\,s^{-1}$
PBIM	d	1.6×10^{-17}	2.8	
PBIM	an	1.3×10^{-17}	2.9	
PBIM	MeOH	1.2×10^{-17}	2.9	
FBIM	an	2.3×10^{-17}	2.6	
Cl-BIM	d	1.3×10^{-17}	2.8	
Me-BIM	d	1.5×10^{-17}	2.7	
OMe-BIM	d	9.0×10^{-18}	3.1	
DI-PBIM	d	7.0×10^{-18}	3.6	
DI-PBIM	an	8.0×10^{-19}	10.7	
DI-PBIM	DMF	1.0×10^{-18}	9.3	
SAM	DMF	4.0×10^{-18}	1.9	

[a] DMF = dimethylformamide; d = dioxane; an = acetonitrile; MeOH = methanol

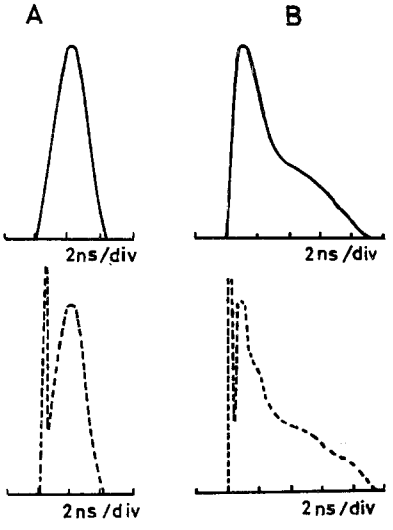

Fig. 6A, B. The experimental (——) and calculated (----) temporal profile of the dye laser pulse. **A** SAM in dimethylformamide. **B** DI-PBIM in dimethylformamide. The initial spike in the calculated pulse is a numerical artefact (see text for details)

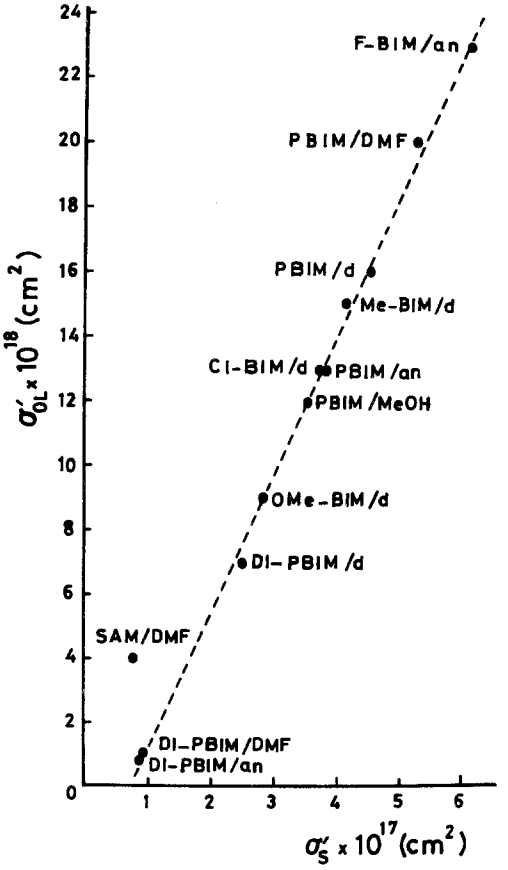

Fig. 7. A graphical presentation of the minimum value of the computed absorption cross section σ'_{OL} that is consistent with the experimental stimulated emission cross-section σ'_S and pulse shape for each laser dye. DMF = dimethylformamide, d = dioxane, an = acetonitrile, MeOH = methanol

studied here. Hence, we arrive to the interesting conclusion that in the solutions of salicylamide and benzimidazole derivatives the lifetime τ'_{S_0} of the ground state tautomer, should be in the range of 6–8 ns.

The direct measurement of reverse proton transfer rates in the ground state ($k'_{S_0S_0}$) is probing to be very demanding; for example values of the ground state tautomer lifetime ranging from 30 ps up to 16 μs have been determined recently [20, 21] for the same compound (3-hydroxyflavone). There are no previous experimental data on τ'_{S_0} for the compounds studied here, although for the related compounds HBO and HBT Itoh and Fujiwara [18] determined S'_0 lifetimes of 260 ns and 9–50 μs respectively. These values have been revised in more recent work, where lifetimes in the subnanosecond (HBO, [15]) and nanosecond (HBT, [16]) range are proposed. The solutions of this kinetic model clearly place the ground state back proton-transfer process of SAM and PBIM derivatives into the nanosecond-subnanosecond time interval. Moreover, it is shown that the physical properties of this transient

state would eventually determine the IPT laser efficiency.

In particular, as the laser pulse width depends critically upon σ'_{OL}, there is a unique correspondence between the (experimental) σ'_S value and the minimum value of σ'_{OL} consistent with the experimentally observed shape of the laser pulse for each compound. This is shown graphically in Fig. 7, where the dashed line joins the pairs of σ'_S, σ'_{OL} values which give rise to laser pulses mirroring the pump pulse. Hence, the laser pulse of SAM fails to follow the pump pulse not because of a low value of the stimulated cross section but due to the absorption losses at the lasing wavelength introduced by σ'_{OL}. In this model the molecular species responsible for that absorption is described as a ground-state keto form. However, it should be recalled that any other transient species absorbing at the laser wavelength and showing a nanosecond lifetime independent of an oxygen concentration in the 0.01 M range would be kinetically equivalent.

Finally, it is interesting to point out that Ernsting and Nikolaus [13] demonstrated numerically and experimentally the use of an ITP dye (HBO) for generating intense picosecond laser pulses. This property was explained by the supression of lasing action due to the accumulation of HBO ground state tautomers in the nanosecond time range.

3. Conclusions

The pulsed operation of salicylamide and phenylbenzimidazole IPT laser dyes can be interpreted with the aid of a four-level kinetic model, built up with the ground and excited states of the normal and tautomer configurations.

According to this model, the laser pulse shape and width depend critically upon the lifetime and absorption cross-section at the lasing frequency of a transient state (the fourth-level) which is assigned here to the tautomer ground state. The losses due to triplet formation, although not negligible, were found not to be the controlling step. For several derivatives of phenylbenzimidazole the small lifetime (<8 ns) and cross section of this transient state might make the use of these compounds in pulsed dye lasers very convenient.

Acknowledgements. J. M. M. and A. D. thank the CSIC for a Scholarship.

This work was done under Projects 653/070 CSIC and 84/145 (CAICYT).

References

1. P. Chou, D. McMorrow, T.J. Aartsma, M. Kasha: J. Phys. Chem. **88**, 4596–4599 (1984)
2. A.U. Acuña, A. Costela, J.M. Muñoz: J. Phys. Chem. **90**, 2807–2808 (1986)
3. A.U. Acuña, F. Amat, J. Catalán, A. Costela, J.M. Figuera, J.M. Muñoz: Chem. Phys. Lett. **132**, 567–569 (1986)
4. A. Costela, F. Amat, J. Catalán, A. Douhal, J.M. Figuera, J.M. Muñoz, A.U. Acuña: Opt. Commun. **64**, 457–460 (1987)
5. J. Sepiol, H. Bulska, A. Grabowska: Chem. Phys. Lett. **140**, 607–610 (1987)
6. A. Weller: Progr. Reaction Kinetics **1**, 187–214 (1968)
7. W. Klöpffer: Adv. Photochem. **10**, 311–358 (1977)
8. A.U. Acuña, J. Catalán, F. Toribio: J. Phys. Chem. **85**, 241–245 (1981)
9. J. Catalán, F. Toribio, A.U. Acuña: J. Phys. Chem. **86**, 303–306 (1982)
10. A.U. Acuña, F. Amat, J. Catalán, A. Douhal, M.P. Lillo: To be published
11. A.J. Kerssley, A.J. Andrews, C.E. Webb: Opt. Commun. **31**, 181–184 (1979)
12. A.U. Khan, M. Kasha: Proc. Natl. Acad. Sci. USA **80**, 1767–1770 (1983)
13. N.P. Ernsting, B. Nikolaus: Appl. Phys. B **39**, 155–164 (1986)
14. F.P. Schäfer: "Principles of dye laser operation". In *Dye Lasers*, ed. by F.P. Schäfer, Topics Appl. Phys. Vol. 1 (Springer, Berlin, Heidelberg 1973) Sect. 1.3, pp. 28–32
15. F. Toribio, J. Catalán, F. Amat, A.U. Acuña: J. Phys. Chem. **87**, 817–822 (1983)
16. T. Elsaesser, B. Schmetzer, M. Lipp, R.J. Bäuerle: Chem. Phys. Lett. **148**, 112–118 (1988)
17. A. Mordzinski, K.M. Grellman: J. Phys. Chem. **90**, 5503–5506 (1986)
18. M. Itoh, Y. Fujiwara: J. Am. Chem. Soc. **107**, 1561–1565 (1985)
19. P. Juramy, P. Flamant, Y.K. Meyer: IEEE J. QE-**13**, 855–865 (1977)
20. T.P. Dzuga, J. Schmidt, T.J. Aartsma: Chem. Phys. Lett. **127**, 336–342 (1986)
21. M. Itoh, Y. Fujiwara: Chem. Phys. Lett. **130**, 365–367 (1986)